Applied Catalysis B: Environmental 187 (2016) 328–341

Contents lists available at ScienceDirect

Applied Catalysis B: Environmental

journal homepage: www.elsevier.com/locate/apcatb

Mobility of gold, copper and cerium species in Au, Cu/Ce, Zr-oxides and its impact on total oxidation of methanol

Piotr Kaminski, Maria Ziolek*

Adam Mickiewicz University in Poznań, Umultowska 89b, 61-614 Poznań, Poland

ARTICLE INFO

Article history:
Received 28 November 2015
Received in revised form 13 January 2016
Accepted 16 January 2016
Available online 19 January 2016

Keywords:
Gold–copper–ceria–zirconia
XPS
UV–vis
Methanol oxidation

ABSTRACT

CeO_2, ZrO_2 and mixed CeZrOx (Ce:Zr = 1:1 assumed) mesoporous oxides were synthesized and used as supports for gold (nominal 1.5 wt%) and copper (nominal 2 wt%). The materials obtained were characterized by UV–vis, XPS and TEM techniques, which allowed monitoring of the oxidation state of metals and surface properties of the catalysts, in particular the concentration of the components on the surface of the solid and in the bulk of the material. The metal-support and metal–metal (in bimetallic Cu-Au samples) interactions were considered. The aim of this work was to investigate the changes in chemical composition of catalyst surfaces and the oxidation states of metals upon the activation of the samples at different temperatures (423 and 573 K) in the argon flow and evaluation of the influence of these changes on the catalytic activity and selectivity in the low temperature oxidation of methanol. It was evidenced that the electronic state of gold and the mobility of metals towards and oxygen from the support play an important role in the low temperature total combustion of methanol. The activation temperature strongly affects the mobility of surface oxygen and the oxidation states of the cationic components playing the role of Lewis acid sites (it causes an increase in Cu^+ and Ce^{3+} species concentration and a decrease in that of cationic gold on the surface after thermal treatment), and therefore strongly affects the activity and selectivity in the oxidation of methanol. The catalysts effective in low temperature total combustion of methanol are proposed.

1. Introduction

Volatile organic compounds (VOCs) belong to hazardous compounds emitted during many industrial technological processes as well as from motor vehicles and they are significant air pollutants. The most ecological, effective and energy saving technique for their abatement is the catalytic combustion to CO_2 and H_2O, preferentially at low temperatures. The reaction of methanol oxidation is one of the model reactions for the removal of VOCs [1,2]. This reaction is also used for testing the surface properties of catalysts based on the products distribution and the knowledge of mechanisms of their formation [2–4]. Supported noble metals or metal oxides are typically used as catalysts for the methanol total combustion. From among metal oxides CeO_2 [5–10], TiO_2 [11,12] or mixed oxide $Ce_xTi_{(1-x)}O_2$ [13,14] are frequently applied in such studies. The noble metals such as Pd, Pt, Ag [15–18] loaded on the supports can act as active sites in this process. Especially effective is the use of nanoparticles of gold supported on the different materials. The application of gold in heterogeneous catalysis was possible after obtaining Au supported nanoparticles whose mean diameter was <5 nm [19]. The gold particles supported on transition metal oxides can be used as catalysts in low temperature oxidation. It is known that Au/CeO_2 system is effective not only in the total combustion of methanol [1] but also in many other catalytic oxidation processes, as e.g. the low temperature CO oxidation [20]. Ceria belongs to the oxides which easily interact with other metals and thanks to this interaction enhances the redox properties [21]. Strong interaction of gold particles was observed on different metal oxide supports, as Co_3O_4, CeO_2, TiO_2, FeO_x [22–25]. If ceria and gold particles were loaded on mesoporous silica, SBA-15, the interaction between CeO_2 and Au particles stabilized the ionic gold species and the dispersion of gold nanoclusters [21,26] especially under the conditions applied in CO oxidation. To enhance the catalytic properties, copper species are sometimes loaded on the support in the vicinity of gold species. In such a case, additional interaction between copper and gold changes the redox and acidic properties of the catalyst surface [26–30]. The interactions mentioned depend strongly on the pre-treatment of the material. For example, for Au-Cu loaded on titania [31] when the calcination temperature was increased, the surface Au/Cu atomic ratio decreased and copper was oxidized. The

* Corresponding author.
E-mail address: ziolek@amu.edu.pl (M. Ziolek).

http://dx.doi.org/10.1016/j.apcatb.2016.01.040
0926-3373/

increase in calcination temperature to 773 K or higher led to the formation of Au-Cu alloy nanoparticles. Mild temperature conditions (673 K) were the best to obtain the catalyst for propene epoxidation, because a strong alloy-support interaction took place at this temperature and small particle size was maintained. In this way a large number of active sites at the perimeter of the contact area between the alloy nanoparticles and TiO_2 was generated. The synergistic effects on the catalyst surface can be enhanced not only by the admission of the second metal species on the support (like the above mentioned bimetallic system Cu-Au), but also by modification of the support oxide as a result of formation of mixed metal oxides. Different examples in literature show e.g. the enhancement of the redox properties by the use of mixed oxides, e.g.: $Ce_xTi_{(1-x)}O_2$ [13,14], $Ce_{1-x}Cu_xO_{2-\delta}$ [32], Al_2O_3-CeO_x [33,34], Cu O-CeO_2/Al_2O_3 [35] or $CeZrO_x$ [28,29,36]. Zirconia is a metal oxide which is characterised by amphoteric properties and with the typical redox oxide, CeO_2, it forms a composition showing acidic and redox properties important for the oxidation of methanol [37]. The presence of Zr^{4+} in mixed cerium-zirconium oxides can lead to the increase in the oxygen mobility of ceria as well as the increase in its reducibility, and it can promote the reduction of noble metals, e.g.: Pt, Rh [38,39].

Au and CeO_2 containing catalysts, supported on SBA-15 mesoporous molecular sieves and loaded with additives such as Cu and Zr species, have been obtained and characterised in our previous paper [29]. It was found that gold and copper loaded on supports strongly interacted with each other which resulted in the electron transfer from copper cations to metallic gold, thus enhancing redox properties. Moreover, cerium species interact with gold, increasing the redox properties of the system. By combination of different compositions of the materials described in that paper it was possible to obtain catalysts selective to the desired products of the oxidation of methanol. For a better insight into the observed behaviour, mesoporous cerium and zirconium oxide systems were applied in this study as supports for gold and copper and the obtained materials were used in the oxidation of methanol in the gas phase.

Before the oxidation performed in the gas phase, thermal activation of the catalysts is necessary. The question arose if the Cu, Au/Ce, Zr—oxide catalysts exhibit the same surface properties after activation in the inert gas atmosphere as the not pre-treated materials. To answer this question, the focus in this paper was on the role of the activation temperature (423 and 573 K) on the surface properties and catalytic activity in methanol oxidation. The oxidation of methanol was used as a test reaction to investigate the role of the metal, the support and the metal-support interaction. The main aim of this work was to investigate the changes in chemical composition of the catalyst surface that resulted from the thermal treatment and their impact on the catalytic activity and selectivity in methanol oxidation with particular emphasis on total combustion of alcohol. For this purpose, the mesoporous ceria, zirconia and mixed cerium-zirconium oxides modified with gold and/or copper were prepared, characterised using selected analytical techniques and investigated in the reaction of methanol oxidation with oxygen in the gas phase.

2. Experimental

2.1. Preparation of catalysts

2.1.1. Synthesis of ceria CeO_2

The synthesis of mesoporous ceria, CeO_2 was carried out with the use of a solution of organic copolymer—Pluronic P-123 (polyethyl glycol-polypropyl glycol-polyethyl glycol, Sigma-Aldrich) in ethanol (POCh). A portion of 1.2 g 0.0002 mol of Pluronic P-123 was dissolved in 12 cm^3 of ethanol. P123 was mixed with ethanol at room temperature for 1 h. Then a powder of metal precursor −25.2307 g (0.0581 mol) of cerium(III) nitrate ($Ce(NO_3)_3{\cdot}6H_2O$, ≥99.99%, Sigma-Aldrich) was added to this mixture which was stirred for 1 h at room temperature. The surfactant/precursor molar ratio was 0.0034. After mixing, a clear colourless solution was obtained. The solution was transferred to a Petri dish (Ø = ∼20 cm), and dried at 323 K for 24 h. The final material was obtained by heating the sample at 673 K for 10 h (a heating rate of 1 K min^{-1}). The catalyst was in the form of yellow powder.

2.1.2. Synthesis of zirconia ZrO_2

Zirconia was synthesized by the hydrothermal method using a surfactant as a structure directing agent [40–43]. A micellar solution of cetyltrimethylammonium bromide (CTMABr, Sigma-Aldrich) was prepared by dissolving the surfactant at room temperature for 3 h in an aqueous acidic solution (pH = 2 controlled by 35–38% HCl, Chempur). Zirconium *n*-tetrapropanol ($Zr(OC_3H_7)_4$, 70% in 1-propanol, Fluka) was added dropwise to the solution of the surfactant to reach the surfactant/precursor molar ratio of 0.33. The gel obtained after stirring for 1 h at 313 K was sealed into a polypropylene bottle and heated for 24 h at 353 K. The template was removed by extraction in Soxhlet apparatus at 351 K using ethanol for 30 h. Then, the oxide was dried in a vacuum rotator at 343 K (200–300 mbar) and calcined at 673 K for 4 h at a heating rate of 3 K min^{-1}.

2.1.3. Preparation of mixed cerium-zirconium oxide, CeZrOx

The mixed oxide, CeZrOx, was synthesized according to the literature method [40–43] using an aqueous acidic solution (pH = 2 controlled by 35–38% HCl, Chempur) of 15 wt% cetyltrimethylammonium bromide (CTMABr, Sigma-Aldrich) by dissolving CTMABr at 313 K under stirring for 3 h. Zirconium *n*-tetrapropanol ($Zr(OC_3H_7)_4$, 70% in *n*-propanol, Fluka) and powder of cerium(III) nitrate ($Ce(NO_3)_3{\cdot}6H_2O$, ≥99.99% Sigma-Aldrich) in the amounts needed to get the assumed CeO_2:ZrO_2 ratio of 1:1, were added into the above-mentioned solution of a surfactant/precursors molar ratio of 0.33. After further stirring for 1 h at 313 K, the mixture was heated at 353 K for 24 h. The template was removed by extraction in a Soxhlet apparatus at 351 K using ethanol for 30 h. Then, the mixed oxide was dried in a vacuum rotator at 343 K (200–300 mbar) and calcined at 673 K for 4 h at the heating rate of 3 K min^{-1}.

2.1.4. Modification of mesoporous oxides with gold

A portion of 4.500 g of dried material (ceria, zirconia or ceria-zirconia oxides) was modified according to the literature method [34,44,45]. A portion of 137 mg of tetrachloroauric acid ($HAuCl_4{\cdot}3H_2O$, Johnson-Matthey, needed to achieve nominal 1.5 wt% of gold loading) was added to 217 cm^3 of distilled water. Then aqua solution of urea (99%, Fluka, 0.16 mol dm^{-3}) was added. The molar ratio of urea/gold was 100. The solution (pH = 2) was stirred in a quartz flask for 4 h at 353 K. Then the product was filtered and washed with 100 cm^3 of aqua solution of ammonia (25%, $NH_3{\cdot}H_2O$, Chempur) and 850 cm^3 of distilled water to reach pH = 7 and remove chlorides. The product was dried at room temperature for 24 h and the final material was obtained after calcination at 623 K for 3 h. Thus, three gold catalysts: Au/CeO_2, Au/CeZrOx and Au/ZrO_2 were made.

2.1.5. Introduction of copper by incipient wetness impregnation

Copper was introduced on the supports by incipient wetness impregnation to get the nominal 2.0 wt% of copper. Before impregnation, the support was dried using a vacuum rotator (200–300 mbar) at 343–348 K for 1 h. The source of copper, i.e. 0.146 g of copper(II) nitrate $Cu(NO_3)_2{\cdot}2.5H_2O$ (Sigma-Aldrich) was dissolved at room temperature in 2 cm^3 of distilled water and used to fill the oxide pores. The wetted oxide was dried under vacuum

at 343 K for 1 h, then at 333 K for 16 h, at atmospheric pressure. The materials were calcined in an oven at 623 K for 3 h (a heating rate of 3 K min^{-1}). The following catalysts were obtained: Cu/CeO_2, Cu/CeZrOx and Cu/ZrO_2.

2.1.6. Modification of gold-containing samples with copper species

The introduction of copper into the samples containing gold was performed by *incipient wetness impregnation*, according to the above described procedure.

2.1.7. Activation of catalysts

Before UV–vis and XPS measurements and oxidation of methanol, the samples were activated in the flow of argon (Linde 5.0 N). At the beginning, the samples in the form of powder were pressed (<2 MPa), crushed and the fraction of particles from 0.5 to 1.0 mm was collected to be used in the reaction. The 0.100 g of the sample was put into the flow-bed reactor (length l = 70 mm and Ø = 5 mm) and the catalyst was heated from room temperature to 423 or 573 K at a rate 10 K min^{-1} in argon flow (40 cm^3 min^{-1}). Then the sample was activated for 1 h in argon flow at a selected temperature.

2.2. Characterisation of catalysts

2.2.1. ICP-OES

In order to establish the metals content, the ICP technique (Varian ICP-OES VISTA-MPX equipment) was applied. Prior to analysis, the accurately weighted catalyst portion (between 30–60 mg) was treated first in aqua regia and brought to reflux. Next sulphuric acid was added to obtain totally dissolved material. After the following addition of distilled water the solution was analysed by ICP-OES.

2.2.2. X-ray diffraction (XRD)

XRD measurements were carried out on a Bruker AXS D8 Advance diffractometer with Cu $K\alpha$ radiation (λ = 0.154 nm), with a step size of 0.5° in the wide-angle range (21–81°).

2.2.3. Ultra-violet spectroscopy (UV–vis)

UV–vis spectra were recorded for calcined catalysts and materials thermally treated according to Section 2.1.7. Contrary to the experiment described in the previous paper [26], the samples were not dried at 383 K overnight (13 h) before the use for UV–vis measurements. The spectra were recorded on a Varian-Cary 300 Scan UV–vis spectrophotometer. Powder samples were put into a cell with a quartz window. The measurements were conducted in the range of 800–190 nm. Spectralon™ was used as the reference material.

2.2.4. X-ray photoelectron spectroscopy (XPS)

Photoelectron spectra were recorded using an Ultra High Vacuum (UHV) System (Specs, Germany). The study was conducted using X-ray Al $K\alpha$ = 1486.6 eV with the parameters of the lamp: 14.5 kV, 20 mA. Measurements were carried out in vacuum of approximately 5.0×10^{-9} mbar in the chamber of the analyser. The spectra were recorded for the energy range from 1100 eV to 0 eV in increments of 0.4 eV, the energy transition CAE = 100 eV. The XP spectra for metal species were recorded in increments of 0.1 eV, at the energy transition CAE = 30 eV and time counts 50 ms. The number of scans of the range measured was chosen to correspond to a given signal to noise ratio. The powder sample was put on the conductive tape, which was adhered to the carrier surface and positioned in perpendicular to the axis of the analyser. The X-ray source was set at an angle of 60° to the plane of the surface. The area of the samples analysed corresponded to the size of the aperture of the analyser used (large area), ca. 50 mm^2. Deconvolution of XP spectra was carried out using OMNIC 8.0™ software. Band intensities were estimated by calculating the integral of each band after smoothing and baseline correction, then set the deconvolution parameters for the experimental curve using the software—Voigt function, signal sensitivity: small and base line: linear Atomic ratios were computed from the intensity ratios normalised by atomic sensitivity factors. An estimated error of ±0.1 eV can be assumed for all measurements.

2.2.5. Transmission electron microscopy (TEM)

Before the measurements using a transmission electron microscopy (TEM), the catalysts in the form of suspension in 1-butanol were deposited on a grid covered with a holey carbon film. The samples were transferred to a JEOL 2000 electron microscope operating at 80 kV. The size distribution and average size of gold particles were estimated using ImageJ software. The precision of particle size determination was ca. ±0.5 nm. Finally, the fractions of gold particles of the same size in all gold particles were calculated to determine the particle size distribution.

2.3. Oxidation of methanol

The methanol oxidation was performed in a fixed-bed flow reactor (Ø = 5 mm and length l = 70 mm). The catalyst powder was pressed, crushed and sieved to the fraction of 0.5 < Ø < 1.0 mm. A portion of 0.100 g of the catalyst was placed into the reactor. The samples were activated in argon flow (40 cm^3 min^{-1}) at 423 or 573 K for 1 h (the rate of heating was 10 K min^{-1}). Then, the temperature was decreased (the rate of cooling was 10 K min^{-1}) to the lowest temperature of the reaction. In the temperature range 353–423 K the reaction was carried out with the use of the same catalyst sample and at increased temperature. At each temperature, the reaction proceeded for 3 h. The reactant mixture of Ar/O_2/MeOH (88/8/4 mol%) was supplied at the rate of 40 cm^3 min^{-1}. Methanol (99.8%, Chempur, Poland) was introduced to the flow reactor by bubbling argon gas through a glass saturator filled with methanol. The reactor effluent was analysed using two online gas chromatographs. One chromatograph, GC 8000 Top, equipped with a capillary column of DB-1, operating at 313 K, with a FID detector applied for analyses of organic compounds and the other, GC containing Porapak Q with a TCD detector together with 5A molecular sieve columns were applied for analyses of O_2, CO_2, CO, H_2O and CH_3OH. The columns in the second chromatograph with TCD were heated according to the following programme: 5 min at 358 K, temperature increase to 408 K (heating rate 5 K min^{-1}), 4 min at 408 K, cooling down to 358 K (for the automatic injection on the column with 5A), 10 min at 358 K, temperature increase to 408 K (heating rate 10 K min^{-1}), 11 min at 408 K. Argon was applied as a carrier gas. The outlet stream line from the reactor to the gas chromatograph was heated at about 373 K to avoid condensation of the reaction products. The selectivity, S_i, was calculated as the molar concentration of the indicated product, i, divided by the sum of the concentrations of all products, $S_i = c_i/\sum c \times 100\%$. The specific catalytic activity (turnover frequency TOF) was calculated as the number of methanol molecules reacted on one Au site (only atoms on the surface of Au particles were considered) in one second. The number of active sites for each catalyst was calculated on the basis of the gold dispersion measured by TEM.

3. Results and discussion

3.1. Characterisation of the catalysts

The wide-angle XRD pattern (Fig. S1) of ceria is characteristic of the cubic phase crystal (JCPDS ICDD PDF Card—00-043-1002). Pure zirconia is a mixture of the tetragonal (JCPDS ICDD PDF

Card—00-042-1164) and monoclinic phase (JCPDS ICDD PDF Card—00-007-0343). The XRD pattern of CeZrOx reveals the domination of peaks from the structure of zirconia. Therefore, for this mixed oxide the zirconia structure with a uniform distribution of cerium ions within this phase can be assumed. The lattice parameter of tetragonal zirconia slightly increased from a = 0.3602 and c = 0.5177 nm for pure ZrO_2 to a = 0.3631 and c = 0.5246 nm for mixed CeZrOx.

The surface area of the catalysts depends on the nature of the supports and increases in the following order: CeO_2 (24 m^2/g) < CeZrOx (103 m^2/g) < ZrO_2 (121 m^2/g). Modification with gold and copper only slightly decreases the surface area of monometallic oxide supports, whereas the catalysts based on CeZrOx (Ce:Zr molar ratio of 0.8 in the bulk – ICP results and 0.9 on the surface – XPS results) reveal much lower surface area (about 65 m^2/g) after modification with Cu and Au.

The surface properties were studied by UV–vis and XPS spectroscopies, TEM images of selected samples were analysed.

3.1.1. UV–vis spectroscopy

UV–vis spectroscopy is a very sensitive probe for the oxidation state and coordination of metals. Fig. 1 shows the UV–vis spectra of the parent materials, fresh catalysts and the materials activated at 423 and 573 K. The bands present in the range between 200 and 400 nm originate from charge transfer (CT) from ligand to cerium cations. The spectrum of CeO_2 shows two well- resolved bands at ca. 265 and 345 nm characteristic of the charge transfer from oxygen ion to cerium cation. The position of the band coming from ligand to metal charge transfer depends on the symmetry of ligand field surrounding the Ce centre [24,46]. The charge transfer from oxygen ions to cerium cations requires higher energy of tetracoordinated cerium cations than that of e.g. hexacoordinated or octacoordinated species. Moreover, the energy of charge transfer depends on the oxidation state of cerium. On the basis of these data, the UV–vis band at ca. 335–350 nm observed in Fig. 1 can be assigned to LMCT for Ce^{4+} with a higher coordination number than 4, whereas the band at ca. 265 nm can be due to O^{2-} to Ce^{4+} tetrahedrally coordinated. The typical band resulting from the charge transfer to Ce^{4+} (at ca. 220 nm) is covered by that at 265 nm and its presence can be deduced from the presence of a shoulder at ~220 nm. The shape of the spectra after modification of ceria with gold and copper does not change, but the intensity of the bands decreases. For CeZrOx support, the only one UV–vis band at 268 nm is visible with a shoulder at ca 220 nm indicating that in the ceria-zirconium mixed oxide the composition of oxidation states and coordination of cerium on the surface differs from that observed on pure ceria. The discussed UV–vis region (200–400 nm) is characteristic not only of the charge transfer between oxygen ions and cerium cations but is also typical of the charge transfer transitions of Au^{3+} and Au^{+} ions with ligands [47–53] or for the absorption bands due to the transition of electrons between molecular orbitals of the few-atomic clusters Au_n (n < 10). Therefore, the examination of this region cannot be useful for characterisation of cationic gold species, while the region of 500–560 nm should be used instead. The bands in this region are characteristic of the optical absorption of light excited oscillating conductivity electrons of metallic gold particles and called "plasmon resonance" [54–58].

Examination of the region above 450 nm gives information about the states of gold and copper. The band between 500 and 560 nm originates from d–d electron transfer in metallic gold [56–58]. From among the spectra of fresh catalysts, such a band is found only in those of the bimetallic (Au-Cu) catalysts, irrespectively of the nature of the support (Figs. 1 and 2). The composition of the support determines the position of this band, it is found at the lowest wavelength if CeZrOx is applied as a support. The deconvolution of this band (Fig. 2) permits identification of three species. Besides the band characteristic of metallic gold (at 544 and 535 nm depending on the nature of the support) revealing the highest intensity, two other bands are present in the spectrum of $CuAu/CeO_2$. According to literature data, the absorption at 626 and 692 nm can be attributed to different origins: LMCT (ligand to metal charge transfer) transitions in copper oxides nanoclusters [59,60], LMCT in $(Cu—O—Cu)^{2+}$ clusters [61–63] and/or inter-valence CT transitions between Cu and other metal ions in the bulk solid solution [64] or $2E_g - 2T_{2g}$ transitions of Cu^{2+} ions in an octahedral O_h configuration [61,63]. Polymeric $Cu^{+}\cdots O^{2-}\cdots Cu^{+}$ is also identified in the spectrum of CuAu/CeZrOx by the band at 639 nm. These results demonstrate the role of the composition of the support on the formation of gold and copper species in bimetallic catalysts.

The thermal activation of the catalysts in argon flow significantly changes the spectra in the region considered. The bands coming from d–d electron transfer in metallic gold become well visible also in the spectra of monometallic (Au) samples, and if the higher activation temperature (573 K) is applied, the intensity of this band for monometallic samples increases and becomes much higher than in the spectra of bimetallic samples based on both, CeO_2 and CeZrOx supports. Thus the changes on the catalysts surfaces resulting from the thermal treatment in the presence of inert gas, i.e. under the reduction conditions, are evidenced. The decrease in the amount of gold species on the surface upon thermal treatment was documented by XPS study, which allows also more precise determination of the oxidation states of the modifiers and the concentration of metals and oxygen on the surface.

3.1.2. XPS study

The results of XPS study provide information about changes in the chemical composition of external surface resulting from the activation of the samples in argon flow at 423 or 573 K. Table 1 shows the distribution of chemical elements before and after the activation of the samples modified with gold and/or copper. It is clear that the activation at the higher temperature in the inert gas significantly influences the surface composition. The amount of cerium cations on the surface considerable increases after heating at both temperatures. Heating at 423 K is sufficient for substantial migration of cerium from the bulk to the external surface. Such migration goes along with the much higher content of the reduced forms of cerium, Ce^{3+}, than those of Ce^{4+}, which results in a decrease in Ce^{4+}/Ce^{3+} ratio (Table 1). As concerns the cerium species in the supports, their two oxidation states, Ce^{3+} and Ce^{4+}, are characterized by XP spectra of Ce $3d_{5/2}$ and assigned on the basis of binding energy (BE) values [65,66]. The discussed migration of cerium cations is accompanied by the movement of oxygen species in the opposite way, i.e. from the surface to the bulk of the material, which was estimated by a decrease in the oxygen content, calculated from XP spectra, after heating. Such mobility of cerium and oxygen leads to the formation of oxygen defects on the catalyst surface. It occurs on all the catalysts containing cerium. The migration of zirconium depends on the composition of the catalysts. For Au/ZrO_2 and Cu/ZrO_2, the concentration of zirconium species on the surface slightly grows after thermal activation, whereas the zirconium in CeZrOx matrix does not migrate on heating if Au is loaded, whereas it migrates into the bulk if copper is loaded. Thus, the mobility of zirconium seems to be dependent on the nature of the modifier (Cu or Au) and it occurs in the vicinity of copper species. The occurrence of bimetallic system (Cu-Au) causes the thermal movement of zirconium in the opposite way i.e. from the bulk to the surface.

The concentration of gold and copper (in monometallic samples) on the surface of ceria, estimated from XP spectra, decreases with increasing activation temperature (Table 1). Such a decrease can be caused by the migration of metals into the bulk of material. The migration of gold seems to be partially protected by

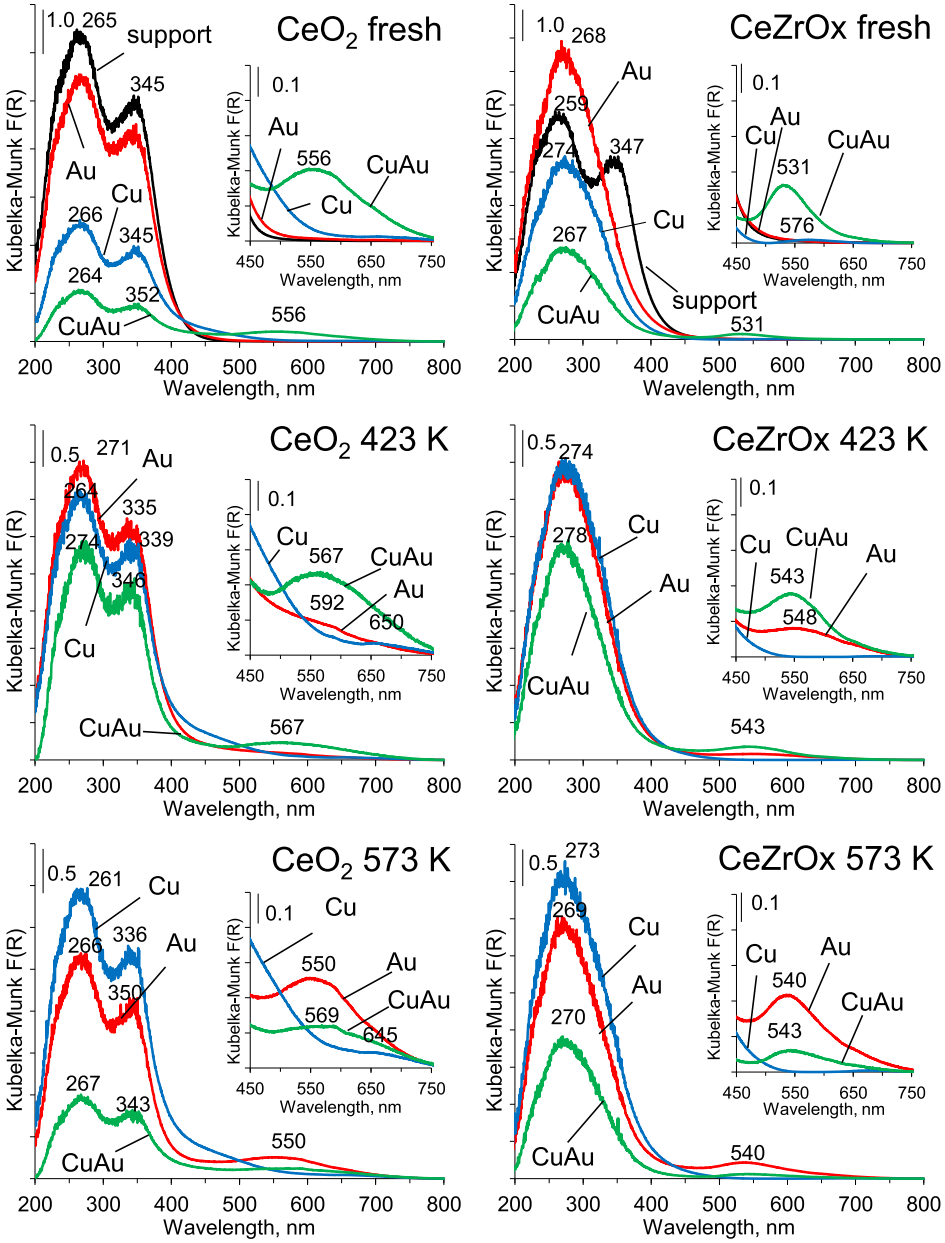

Fig. 1. UV–vis spectra of CeO_2 and CeZrOx before activation and after activation at 423 or 573 K. Mesoporous oxides are marked by black line, Au catalysts—red line, Cu catalysts—blue line and Cu-Au catalysts—green line. (For interpretation of the references to color in this figure legend, the reader is referred to the web version of this article.)

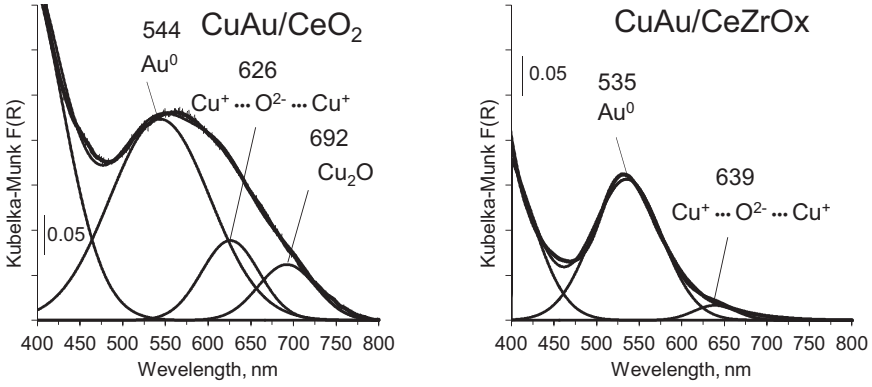

Fig. 2. UV–vis deconvoluted spectra in the 400–800 nm range of fresh bimetallic catalysts based on CeO_2 and CeZrOx.

Table 1
Distribution of elements on the catalyst surfaces – calculated from XPS results.

Catalyst	Distribution of elements, atomic%					Cationic ratio	
	Au	Cu	Ce	Zr	O	Cu^{+}/Cu^{2+}	Ce^{4+}/Ce^{3+}
Au/CeO_2 before activation	4.9	–	57.6	–	37.5	–	2.5
Au/CeO_2 act. 423 K	3.0	–	76.3	–	20.7	–	1.5
Au/CeO_2 act. 573 K	1.5	–	75.3	–	23.2	–	1.6
Cu/CeO_2 before activation	–	3.7	23.0	–	73.3	1.4	1.5
Cu/CeO_2 act. 423 K	–	2.8	72.0	–	25.2	5.8	1.9
Cu/CeO_2 act. 573 K	–	2.6	74.4	–	23.0	5.7	1.5
$CuAu/CeO_2$ before activation	2.4	2.5	30.1	–	65.0	5.1	3.3
$CuAu/CeO_2$ act. 423 K	1.0	2.1	72.3	–	24.6	4.5	3.0
$CuAu/CeO_2$ act. 573 K	1.4	3.2	72.2	–	23.3	6.1	2.1
Au/CeZrOx before activation	2.9	–	15.8	29.8	51.4	–	3.1
Au/CeZrOx act. 423 K	2.2	–	33.1	28.9	35.8	–	1.4
Au/CeZrOx act. 573 K	1.7	–	38.4	29.7	30.2	–	2.5
Cu/CeZrOx before activation	–	1.1	17.8	32.8	48.3	7.5	1.3
Cu/CeZrOx act. 423 K	–	1.6	36.0	23.7	38.7	1.1	1.8
Cu/CeZrOx act. 573 K	–	1.3	35.6	26.2	36.9	3.2	1.4
CuAu/CeZrOx before activation	3.0	1.7	14.7	14.3	66.3	10.3	4.5
CuAu/CeZrOx act. 423 K	1.4	2.3	35.8	28.2	32.2	2.8	1.8
CuAu/CeZrOx act. 573 K	1.8	2.2	40.0	21.1	34.8	1.7	1.8
Au/ZrO_2 before activation	0.7	–	–	47.3	52.0	–	–
Au/ZrO_2 act. 423 K	0.9	–	–	55.6	43.5	–	–
Au/ZrO_2 act. 573 K	3.0	–	–	54.3	42.7	–	–
Cu/ZrO_2 before activation	–	0.9	–	48.4	50.8	5.6	–
Cu/ZrO_2 act. 423 K	–	1.3	–	53.0	45.7	1.5	–
Cu/ZrO_2 act. 573 K	–	1.6	–	53.1	45.3	0.6	–

the use of mixed CeZrOx as a support instead of pure ceria. The Au content on the surface of Au/CeZrOx after activation at 573 K decreases to 1.7 at.% (from 2.9 at.%), whereas on Au/CeO_2 – to 1.5 at.% (from 4.9 at.%). In contrast, on the surface of Au/ZrO_2 after the thermal activation the content of gold species increases (i.e. shows the opposite behaviour to all the other samples characterised in Table 1). The oxygen content on the surface of this catalyst decreases with increasing activation temperature, but the drop in its concentration is not so high as for the samples based on ceria and mixed oxide, CeZrOx.

The above presented analysis of the elements distributed on the surface of the catalysts shows that the catalytic systems applied in this work are dynamic and upon heating in the inert atmosphere there is a general tendency to the enrichment of the surface in cerium species and a decrease in the content of Au, Cu, and Zr on the surface accompanied by a decrease in the content of oxygen ions on the surface. However, not only the content of all elements on the surface and in the bulk are important for the catalytic activity but also the oxidation states of all components. The distributions of different gold and copper species are shown in Tables 2 and 3, whereas the cationic ratios of copper and cerium are given in Table 1.

The presence of copper lowers the amount or eliminates the presence of cationic gold species and enhances the appearance of negative charge on the metallic gold nanoparticles $(Au^0)^{\delta-}$. The abundance of copper in +1 oxidation state (BE of Cu $2p_{3/2}$ = 931–933 eV) was dominant. Binding energy of ligand to metal charge transfer (LMCT) in Cu^{2+} is observed in the range of 933.5–935.5 eV [31,67–69] and the BE value depends on the chemical composition of the catalysts. The contents of both copper species depend on the activation temperature, but the trends of changes are not the same for all the samples, because they depend on the chemical composition of the catalysts. One of the lowest Cu^{+}/Cu^{2+} ratios (1.39) is observed for the fresh Cu/CeO_2 but the content of Cu^{2+} species is the highest for this sample. The concentration of Cu^{+} on the surface of Cu/CeO_2 increases after the thermal activation in the inert gas (reduction atmosphere). It is accompanied by a significant decrease in the content of Cu^{2+} suggesting the preferential movement of copper species at the higher oxidation state. If Au is added to the system ($CuAu/CeO_2$), the concentration of Cu^{2+} in the fresh sample is low and it does not change considerably upon heating. It means that Au-Cu interaction influences the migration of copper. The application of mixed oxide (CeZrOx) as a support for copper leads to the opposite phenomenon, i.e. a slight change in the Cu^{+} concentration on the surface and the increase of Cu^{2+} after activation, which result from Cu-Zr interaction. According to literature [34,70] the binding energy (BE) of Au $4f_{7/2}$ for bulk metallic gold Au^0 is 83.0–84.4 eV, for Au^{+}—84.5–85.0 eV and for Au^{3+}—85.0–86.5 eV. It is very difficult to distinguish Au^{+} and Au^{3+} species because the above-presented limits of BE ranges are not rigid. The values of BE of Au $4f_{7/2}$ shown in Table 2 oscillate between 82.0 and 86.1 eV, i.e. The values below 83.0 eV cannot originate from plasmon resonance in metallic gold and they are assigned to negatively charged metallic gold particles, $(Au^0)^{\delta-}$ [31,71,72]. Such species in the fresh samples are present only in bimetallic CuAu/CeZrOx, i.e. the multicomponent system containing not only two different metal species (Cu, Au) loaded on the support but also two metal components in the support (Ce, Zr). Due to the synergistic interactions of all these components, especially metallic gold with the more abundant Cu^{+}, electrons are easily transported to the surface of metallic gold nanoparticle. This electron transfer can be stimulated by heating in the inert atmosphere, giving rise to the formation of $(Au^0)^{\delta-}$ species also on pure ceria support after activation at 423 and 573 K. (Table 2). Such an electron transfer is inhibited by the presence of zirconium in the support if copper is not present in the catalyst (monometallic gold samples). $(Au^0)^{\delta-}$ species are formed on CeZrOx support in the vicinity of copper. One cannot exclude the presence of Au^0 in bimetallic (Cu-Au) particles leading to a decrease in $4f_{7/2}$ BE observed for metallic gold species. However, the same decrease in $4f_{7/2}$ BE was observed for metallic gold present in monometallic sample (Au/CeO_2 act. 573 K). Therefore we assigned it mainly to negatively charged metallic gold particles. The most abundant gold species are metallic gold nanoparticles. Their con-

Table 2
Binding energy of gold species – from XPS, before and after activation at 423 or 573 K.

Catalyst	Binding energy of Au $4f_{7/2}$ eV/atomic%[a]		
	$(Au^0)^{\delta-}$ or Au^0 in bimetallic particles	Au^0	Au^{3+}
Au/CeO_2 before activation	–	83.3/3.79	85.4/1.11
Au/CeO_2 act. 423 K	–	83.0/2.44	84.8/0.56
Au/CeO_2 act. 573 K	82.6/0.16	84.1/1.34	–
$CuAu/CeO_2$ before activation	–	83.6/2.31	85.4/0.09
$CuAu/CeO_2$ act. 423 K	82.6/0.16	83.8/0.84	–
$CuAu/CeO_2$ act. 573 K	82.2/0.17	83.6/1.23	–
Au/CeZrOx before activation	–	84.6/1.99	86.1/0.91
Au/CeZrOx act. 423 K	–	83.5/1.96	85.3/0.24
Au/CeZrOx act. 573 K	–	83.6/1.55	85.7/0.15
CuAu/CeZrOx before activation	82.8/0.57	84.0/2.43	–
CuAu/CeZrOx act. 423 K	82.1/0.13	83.4/1.27	–
CuAu/CeZrOx act. 573 K	82.0/0.25	83.4/1.55	–
Au/ZrO_2 before activation	–	83.7/0.62	85.5/0.08
Au/ZrO_2 act. 423 K	–	83.6/0.84	85.5/0.06
Au/ZrO_2 act. 573 K	–	83.6/2.77	85.9/0.23

[a] Percent calculated in relation to the total number of all atoms reported in Table 1.

tent usually rises, whereas the amount of cationic gold decreases upon heating at 423 and 573 K. Such a phenomenon points out the effect of the thermal activation on the composition of active centres on the surface of the catalyst.

Generally, the surfaces of all catalysts used within this work are rich in Ce^{4+}, Zr^{4+}, Cu^+ and Au^0 species and their content strongly depends on the composition of the catalysts and the thermal treatment. Moreover Cu^{2+}, Ce^{3+}, Au^{3+} and $(Au^0)^{\delta-}$ species are found on the surface. As mentioned in literature [73], cerium and zirconium oxide stabilize the cationic state of gold. In contrast, Cu species lower the concentration of gold in the positively charged states and favour their reduction.

3.1.3. Transmission electron microscopy (TEM)

Transmission electron microscopy was used to estimate the size and distribution of gold particles on the surface of monometallic Au and bimetallic Cu-Au catalysts. The examples of TEM images are shown in Fig. S2. The particle size distributions (PSD) for the selected samples are presented in Fig. 3. Let's consider at first the changes in gold crystallite sizes depending on the chemical composition of the supports. The use of the bimetallic support (CeZrOx) results in a wider PSD and greater mean particle size irrespective of the use of gold alone or together with copper. It can be caused by the different interaction between Au and Ce on the pure ceria and on CeZrOx. Surprisingly, the increase in activation temperature from 423 to 573 K gives rise to a decrease in the mean size of gold crystallites and this effect is independent of the chemical composition of the catalysts. Typically, an increase in the temperature of thermal treatment should lead to greater agglomeration of metallic gold. Instead of such an effect, the gold particle size became smaller. It could be explained by the migration of gold species into the bulk of the material and a decrease in their concentration on the surface. Thus not only the chemical composition of the catalyst surface is modified by the thermal treatment but also its textural properties, i.e. the size of gold crystallites.

3.2. Methanol oxidation

The oxidation of methanol is frequently used as the test reaction [2–4] which allows the investigation of the role of different components in multimetallic catalysts. Over gold-containing catalysts the main reaction path is often combustion of the alcohol yielding H_2O and CO_2 [2]. The other reaction paths are also possible, as partial oxidation of methanol, its steam reforming, decomposition as well

Table 3
Binding energy of Cu species—from XPS, before and after activation at 423 or 573 K.

Catalyst	Binding energy of Cu $2p_{3/2}$, eV/atomic%[a]	
	Cu^+	Cu^{2+}
Cu/CeO_2 before activation	933.0/2.15	934.4/1.55
Cu/CeO_2 act. 423 K	931.7/2.39	934.0/0.41
Cu/CeO_2 act. 573 K	931.4/2.21	933.6/0.39
$CuAu/CeO_2$ before activation	932.0/2.09	934.9/0.41
$CuAu/CeO_2$ act. 423 K	932.5/1.72	935.5/0.38
$CuAu/CeO_2$ act. 573 K	932.6/2.75	935.2/0.45
Cu/CeZrOx before activation	932.0/0.97	934.8/0.13
Cu/CeZrOx act. 423 K	931.6/0.85	934.2/0.75
Cu/CeZrOx act. 573 K	931.4/0.99	933.8/0.31
CuAu/CeZrOx before activation	933.3/1.55	935.0/0.15
CuAu/CeZrOx act. 423 K	932.8/1.69	935.0/0.61
CuAu/CeZrOx act. 573 K	932.6/1.37	935.3/0.83
Cu/ZrO_2 before activation	932.4/0.76	934.2/0.14
Cu/ZrO_2 act. 423 K	932.2/0.77	934.5/0.53
Cu/ZrO_2 act. 573 K	932.1/0.58	934.6/1.02

[a] Percent calculated in relation to the total number of all atoms reported in Table 1.

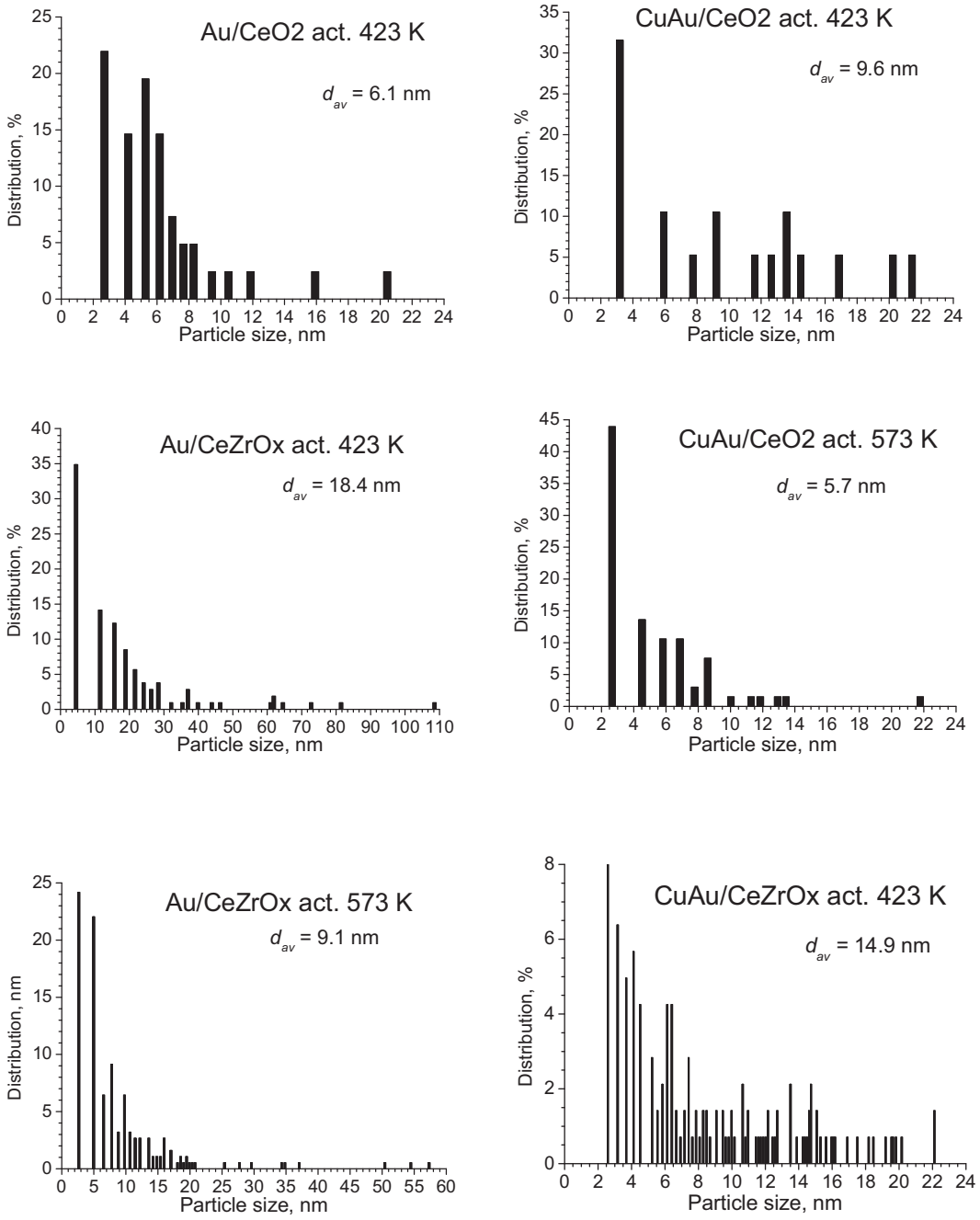

Fig. 3. Gold crystalline size distribution for the selected samples—calculated on the basis of TEM images.

as selective oxidation of methanol towards methyl formate (MF), formaldehyde (FA) and dimethoxymethane (DMM).

In this study, the reaction was performed at low temperatures, ranging between 353 and 423 K (occasionally at a lower temperature) over the catalysts activated in argon flow at different temperatures, 423 and 573 K. The results obtained are shown in Table S1 and Figs. 4–8 . From among all three supports, only CeO_2 exhibits activity after activation at 423 K under the conditions used in this work and a significant selectivity to methyl formate, typical of the redox—acidic catalytic route [2]. One hundred percent selectivity to MF observed at 353 and 373 K (for the sample activated at 423 K) decreases with increasing reaction temperature and FA appears in the reaction products. However, the conversion of methanol is relatively low, the maximum conversion at 423 K reaches 30%. Gold loading on ceria leads to a considerable increase in methanol conversion (above 90% even at 353 K) and the total combustion of methanol (100% selectivity to CO_2 over samples activated at 573 K—Fig. 5). The total combustion of methanol over gold supported on ceria is very well known [1]. In the indicated reference the authors have correlated the high activity of Au/CeO_2 system with the capacity of gold nanoparticles to weaken the Ce—O bond, thus increasing the mobility/reactivity of the surface lattice oxygen which is involved in the volatile organic compounds oxidation through the Mars-van Krevelen reaction mechanism. In view of this, it is clear that electronic state of gold plays an important role in this process as stressed in [73]. As Table 2 shows, the electronic state of gold in the samples studied within this work strongly depends on the composition of the supports and the activation temperature. The mixed cerium–zirconium oxide (CeZrOx) applied as a support for gold gives rise to the higher methanol conversion

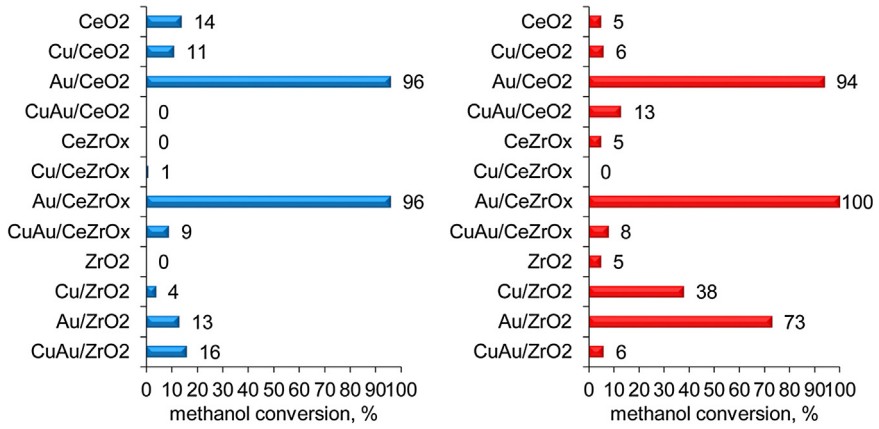

Fig. 4. Methanol conversion at 353 K on the catalysts activated at 423 K (left side) and 573 K (right side) in the argon flow (in the reaction mixture of gases: $Ar/O_2/CH_3OH = 88/8/4\%$ mol, total flow: 40 $cm^3\ min^{-1}$).

(100%) at 373 K over Au/CeZrOx than that observed over Au/CeO_2 catalyst, irrespectively of the activation temperature (Figs. 5 and 7). The Au/CeZrOx sample does not contain negatively charged gold crystallites but only metallic and cationic gold species. Cationic gold species, with the positive charge below +1, have been pointed out by some authors [73] as responsible for the selective oxidation of methanol to formaldehyde. The gold catalysts shown in Table 2 contain Au^{3+} species besides metallic gold and they are not active in the production of formaldehyde but exhibit total combustion activity.

The specific activity expressed by turnover frequency (TOF) calculated per one gold atom on the surface of gold particles (Table 4) indicates that the use of CeZrOx as a support for gold, instead of CeO_2, significantly increases the TOF number from 4.8 s^{-1} to 14.4 s^{-1} for the Au/CeZrOx sample activated at 423 K. The selectivity to CO_2 over Au/CeZrOx is above 90% irrespectively of the activation temperature. The content of gold species on the surface of Au/CeZrOx after activation at 423 K is much lower than on the surface of Au/CeO_2 and the surface area of Au/CeZrOx is higher

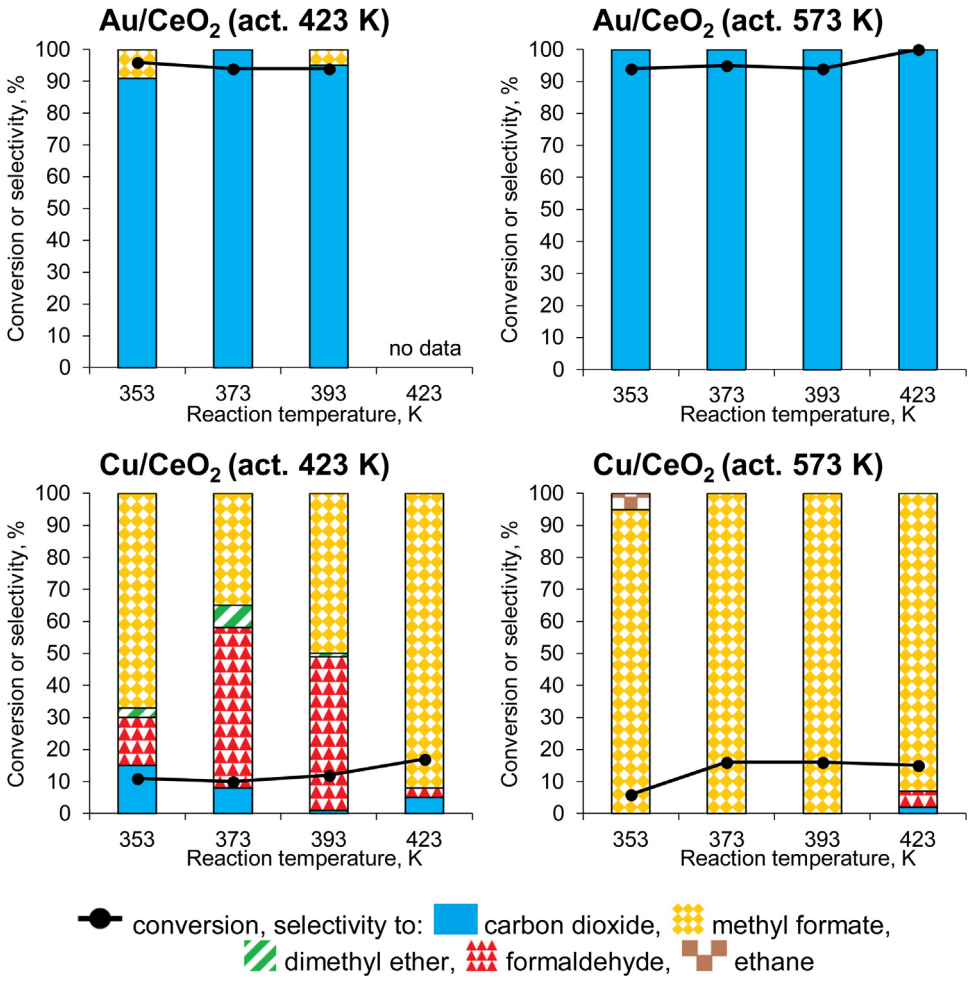

Fig. 5. The results of methanol oxidation over cerium catalysts.

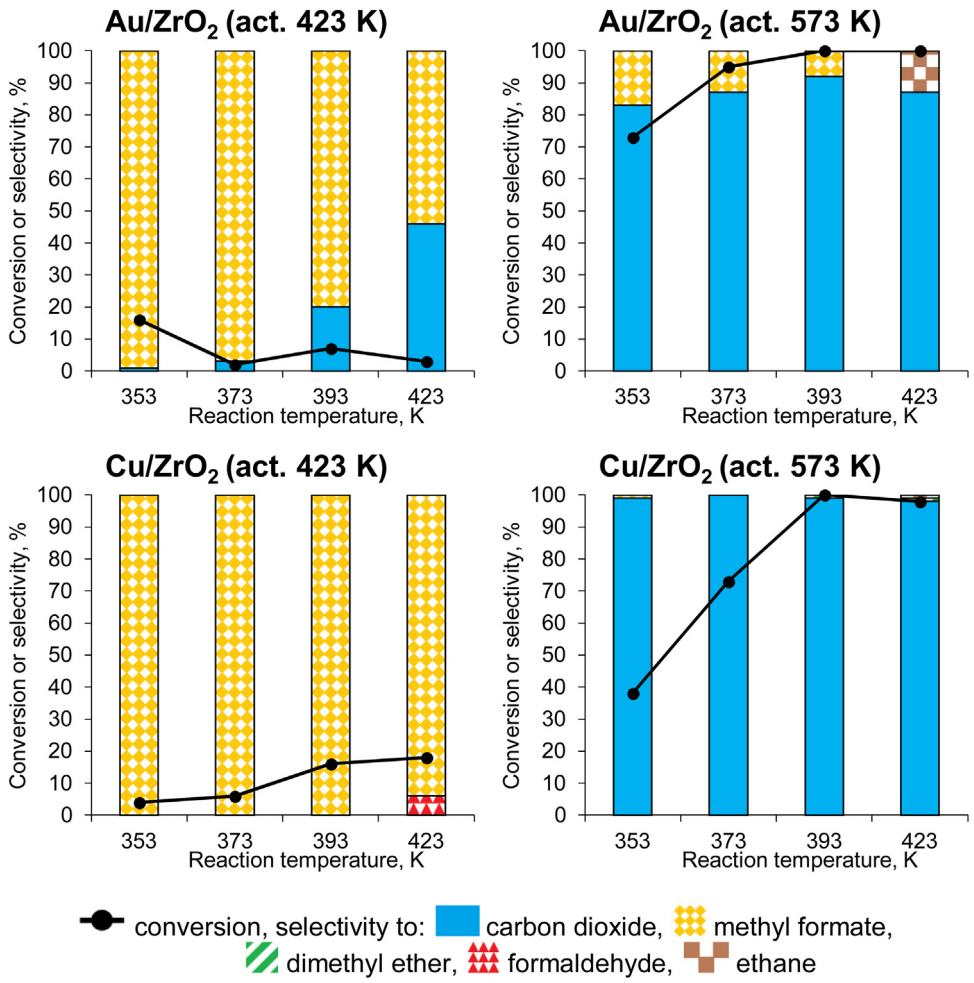

Fig. 6. The results of methanol oxidation over zirconium catalysts.

($65\ m^2\ g^{-1}$) than that of Au/CeO_2 ($25\ m^2\ g^{-1}$). Therefore, the access of reagents to oxygen from the support seems to be much easier. Moreover, the interaction between zirconium and cerium in mixed oxide results in the enrichment of the support surface in mobile oxygen (Table 1) participating in the combustion of methanol [73]. The increase in the activation temperature to 573 K causes the decrease of TOF from $14.4\ s^{-1}$ to $7.4\ s^{-1}$ over Au/CeZrOx. It can be correlated with the decrease in the oxygen content on the catalyst surface, as shown in Table 1.

Monometallic copper catalysts based on CeO_2 are considerably less active than gold catalysts, irrespective of the activation temperature, and exhibit different selectivity (Table S1 and Fig. 5) which depends on the thermal treatment conditions. Cu/CeO_2 activated at 423 K is selective mainly to formaldehyde and methyl formate, whereas the same catalyst activated at 573 K reveals selectivity mainly to MF at all used reaction temperatures. Modification of ceria with copper species evidently must change the strength of Lewis acidity. It is known [2,3] that formaldehyde production requires weak Lewis acid sites to prevent too strong adsorption of the product and a relatively low amount of active oxygen to prevent fast over-oxidation to formic acid, methyl formate and CO_2. Methoxy species bound on the metal oxide surface are reasonable reaction intermediates, whereas strongly bound formate species can act as poison of the reaction. The exclusive production of methyl formate on Cu/CeO_2 activated at 573 K shows that the Lewis acid sites are strong enough to keep formate species and allow them to interact with methanol molecule, but not too strong to prevent the poison of the active sites by formate species. The application of CeZrOx as a support for copper results in a significant decrease in the activity, irrespective of the activation temperature (Fig. 7). Such a support causes greater migration of copper into the bulk

Table 4
TOF calculated for selected catalysts for methanol oxidation at 353 K.

Catalyst	Au content,wt% (from ICP-OES)	Av. size of Au particles, nm(from TEM)[a]	Temp. act.,(K)	Conversion,(%)	TOF[b], (s^{-1})
Au/CeO_2	1.02	6.1	423	96	4.8
$CuAu/CeO_2$	0.96	9.6	423	0	0
Au/CeZrOx	0.97	18.4	423	96	14.4
CuAu/CeZrOx	1.04	14.9	423	9	1.1
Au/CeZrOx	0.97	9.1	573	100	7.4
$CuAu/CeO_2$	0.96	5.7	573	13	0.6

[a] After activation at selected temperatures.
[b] Calculated as the number of methanol molecules reacted on one gold atom on the crystallites surface in one second.

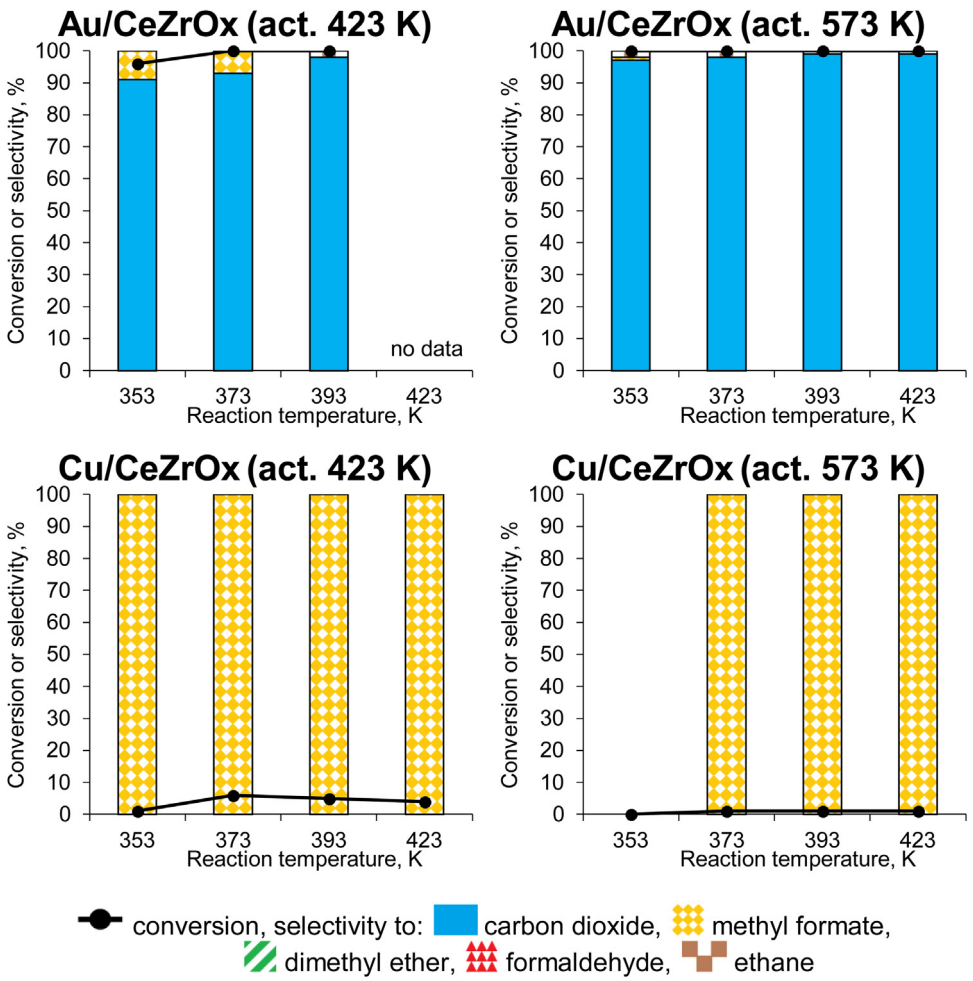

Fig. 7. The results of methanol oxidation over cerium-zirconium catalysts.

of oxides (Table 1) and increases the amount of polymeric copper species ($Cu^{+}\cdots O^{2-}\cdots Cu^{+}$) (Fig. 2).

The effect of the activation temperature of the catalysts on the methanol conversion and selectivity of the reaction is particularly evident on ZrO_2 support. From among all catalysts activated at 423 K, only gold catalysts based on CeO_2 and $CeZrO_2$ exhibit very high methanol conversion (96%) at 353 K (Fig. 4). The increase in the activation temperature gives rise to a significant increase in methanol conversion which achieves 100% at 393 K (Table S1). It is accompanied by a considerable growth of the surface area of gold species on ZrO_2 (Table 1), one of the highest dominations of metallic gold clusters ($Au^0/Au^{3+} = 12$), and the lack of the negatively charged metallic gold particles (Table 2). The significant enrichment of metallic gold species on the surface of Au/ZrO_2 is responsible for the considerable growth in activity in methanol oxidation. The same phenomenon was observed for copper loaded on zirconia in which the substantial increase in the amount of Cu^{2+} species on the surface of the support was noted. The activation temperature influenced the selectivity of the reaction on both catalysts, gold and copper loaded on zirconia. The samples activated at 423 K produce mainly methyl formate, whereas after activation at 573 K the total combustion of methanol to CO_2 distinctly dominates (Fig. 6). Taking into account that total combustion requires strong enough Lewis acidity and high mobility of surface oxygen, one can suggest that the activation temperature strongly affects both features.

Bimetallic, Cu-Au, catalysts on all the three types of support used in this work are less active than the respective monometallic gold catalysts (Table S1, Figs. 4 and 8). Thus the admission of copper species diminishes the activity of gold mainly by the electron transfer from Cu^{+} to metallic gold giving rise to the formation of negatively charged gold clusters (Table 2). This behaviour is independent of the activation temperature.

A comparison of the discussed results of methanol oxidation with those obtained over Cu-Au, Ce, Zr loaded on SBA-15 [29] leads to astonishing conclusions. If ceria and zirconia containing SBA-15 were modified with both, gold and copper, they exhibited high activity at low temperature (423 K) towards total combustion of methanol and their activity was much higher than that of monometallic (gold) catalysts. This phenomenon is in contrast to the results presented in this paper for gold and copper catalysts supported directly on mesoporous cerium and zirconium oxides. The reason is in the different surface properties of both types of catalytic systems. For the catalysts based on mesoporous SBA-15 support, a segregation of ZrO_2 and CeO_2 occurred, ceria moved to the bulk of the material into the mesopores, whereas zirconium species were mostly located on the surface. This phenomenon caused the separation of both oxides. Gold was preferentially placed on the surface and strongly interacted with copper in bimetallic catalysts because ceria hidden in the pores of SBA-15 did not interact with gold. BE for bimetallic, Cu-Au catalysts was higher than for monometallic ones which is in contrast to the observations for the other catalysts presented in this work. Moreover, monometallic samples based on

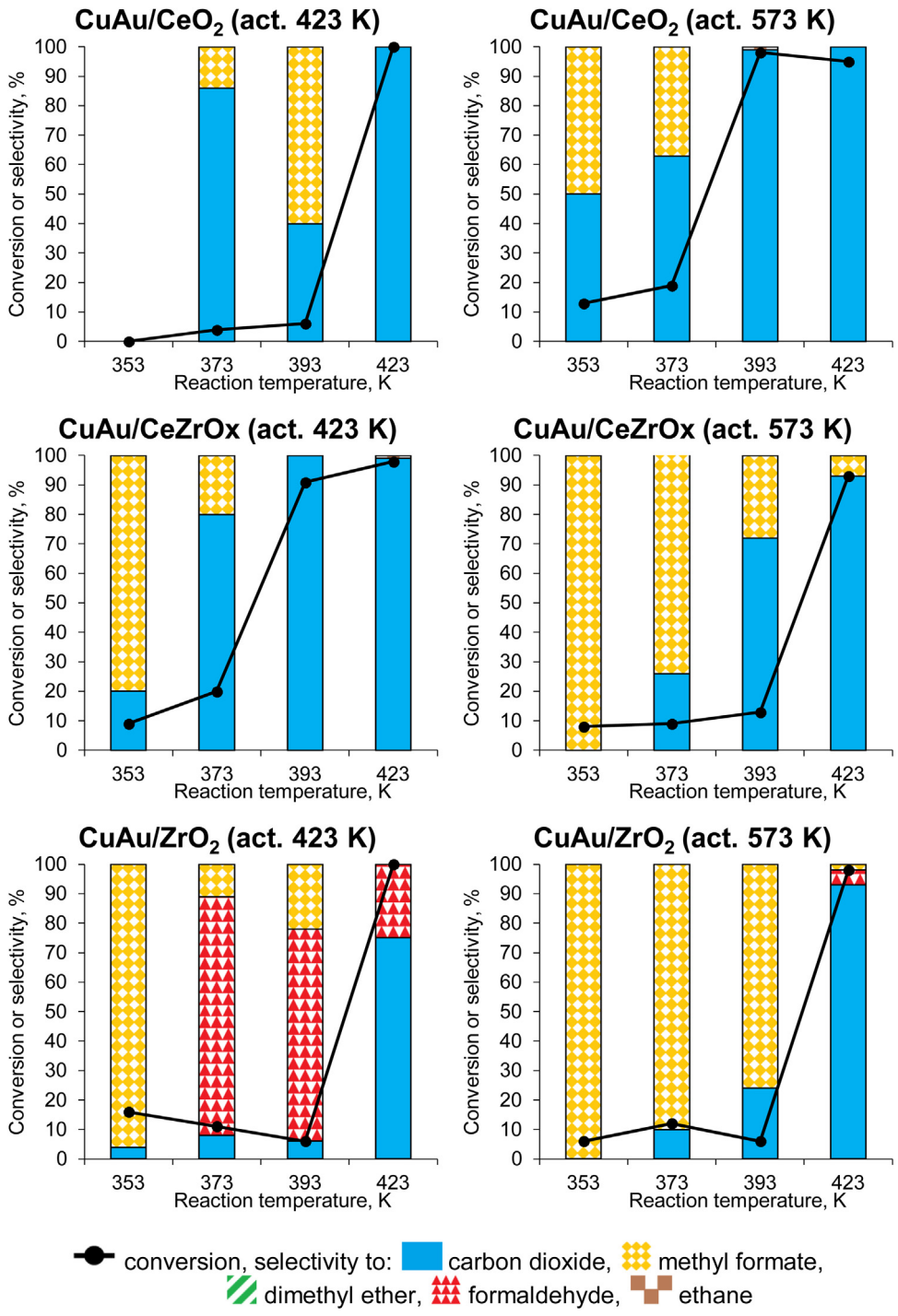

Fig. 8. The results of methanol oxidation over Cu-Au catalysts.

SBA-15 contained only Cu^{2+} copper species and only after addition of gold, part of copper was transformed to Cu^{+} cations, while the application of not dispersed, bulk cerium and zirconium oxides in this work gave rise to both cationic forms of copper with the domination of Cu^{+} even in the monometallic copper catalysts. It means that copper loaded directly on cerium and zirconium oxides interacts stronger with the oxides than with the gold species. The different synergistic interaction between the components of the catalysts based on SBA-15 and those supported on bulk ceria and zirconia oxides, results in their different catalytic activity in the oxidation of methanol.

4. Conclusions

The monometallic (Au or Cu) and bimetallic catalysts loaded on mesoporous ceria, zirconia and mixed ceria-zirconia oxides were characterized after thermal treatment in the inert atmosphere (argon flow) at different temperatures and applied in the oxidation of methanol.

One of the most important finding from this work is the evidence for migration of all the elements building the catalysts depending on the pre-treatment conditions and the chemical composition of the catalysts. Generally, under heating in the inert atmosphere there is a tendency to enrichment of the surface in cerium species

(the migration of cerium from the bulk to the surface) and a decrease in gold, copper and zirconium content on the surface accompanied by a decrease in oxygen ions on the surface. The concentration of gold and copper on the surfaces of the monometallic catalysts decreases with increasing activation temperature. The migration of gold is partially protected by the use of CeZrOx as a support. The migration of copper and cerium in the higher oxidation states, Cu^{2+} and Ce^{4+}, respectively, is favourable and therefore after thermal treatment the surfaces of the catalysts are enriched in Cu^{+} and Ce^{3+} species. The presence of copper in the vicinity of gold particles in the bimetallic catalysts leads to generation of negatively charged metallic gold particles, not present in monometallic gold catalysts. These species are formed by the electron transfer from Cu^{+} to metallic gold and their formation is inhibited by the presence of zirconium in the support. The most abundant gold species are metallic gold nanoparticles and their content increases with increasing of activation temperature because in the same order the amount of cationic gold decreases. The electronic state of gold and the mobility of oxygen from the support play an important role in the low temperature total combustion of methanol. The monometallic gold catalysts based on all the supports used are more active in the low temperature oxidation of methanol than the bimetallic Cu-Au catalysts. The use of CeZrOx support for gold instead of CeO_2 causes an increase in the TOF number by ca. three times if the samples are activated at 423 K. The increase in the activation temperature causes a decrease in the TOF number by ca two times which can be correlated with the decrease in the content of surface oxygen species.

The activation temperature strongly affects the mobility of surface oxygen and the oxidation states of the catalyst components (cations, playing the role of Lewis acid sites) and therefore it strongly affects the activity in the oxidation of methanol and the selectivity of the reaction. The best catalyst in the total combustion of methanol was Au/CeZrOx activated at 573 K which exhibited 100% conversion of methanol and 98% selectivity to CO_2 at 353 K.

Acknowledgment

The authors acknowledge the National Science Centre (Narodowe Centrum Nauki, NCN) in Poland for the financial support (projects No. 2014/13/N/ST5/01282 and 2014/15/B/ST5/00167).

Appendix A. Supplementary data

Supplementary data associated with this article can be found, in the online version, at http://dx.doi.org/10.1016/j.apcatb.2016.01.040.

References

[1] S. Scire, S. Minico, C. Crisafulli, C. Satriano, A. Pistone, Appl. Catal. B: Environ. 40 (2003) 43–49.
[2] K. Kahler, M.C. Holz, M. Rohe, A.C. van Veen, M. Muhler, J. Catal. 299 (2013) 162–170.
[3] J.M. Tatibouet, Appl. Catal. A: Gen. 148 (1997) 213–252.
[4] M. Trejda, J. Kujawa, M. Ziolek, Catal. Lett. 108 (2006) 141–146.
[5] S.Y. Liu, S.M. Yang, Appl. Catal. A: Gen. 334 (2008) 92–99.
[6] Y. Shen, X. Yang, Y. Wang, Y. Zhang, H. Zhu, L. Gao, M. Jia, Appl. Catal. B: Environ. 79 (2008) 142–148.
[7] B.E. Solsona, T. Garcia, C. Jones, S.H. Taylor, A.F. Carley, G.J. Hutchings, Appl. Catal. A: Gen. 312 (2006) 67–76.
[8] D. Andreeva, P. Petrova, L. Ilieva, J.W. Sobczak, M.V. Abrashev, Appl. Catal. B: Environ. 77 (2008) 364–372.
[9] L.F. Liotta, G. Di Carlo, A. Longo, G. Pantaleo, A.M. Venezia, Catal. Today 139 (2008) 174–179.
[10] S. Rojluechai, S. Chavadej, J.W. Schwank, V. Meeyoo, Catal. Commun. 8 (2007) 57–64.
[11] S.Y. Liu, S.M. Yang, Appl. Catal. A: Gen. 334 (2008) 92–99.
[12] S. Damyanova, M.L. Cubeiro, J.L.G. Fierro, J. Mol. Catal. A: Chem. 142 (1999) 85–100.
[13] C. Gennequin, M. Lamallem, R. Cousin, R.S. Siffert, F. Aïssi, A. Aboukaïs, Catal. Today 122 (2007) 301–306.
[14] M. Lamallem, H.E. Ayadi, C. Gennequin, R. Cousin, S. Siffert, F. Aïssi, A. Aboukaïs, Catal. Today 137 (2008) 367–372.
[15] S. Rojluechai, S. Chavadej, J.W. Schwank, V. Meeyoo, Catal. Commun. 8 (2007) 57–64.
[16] V.R. Choudhary, C. Samanta, T.V. Choudhary, Appl. Catal. A: Gen. 308 (2006) 128–133.
[17] F. Menegazzo, P. Burti, M. Signoretto, M. Manzoli, S. Vankova, F. Boccuzzi, F. Pinna, G. Strukul, J. Catal. 257 (2008) 369–381.
[18] T. Tabakova, F. Boccuzzi, M. Manzoli, A. Chiorino, D. Andreeva, C.C. Aldo Gamba, C. Salvatore, Studies in Surface Science Catalysis, 155, Elsevier, New York, 2005, pp. 493–500.
[19] M. Haruta, T. Kobayashi, H. Sano, N. Yamada, Chem. Lett. 16 (1987) 405–408.
[20] M.M. Schubert, V. Plzak, J. Garche, R.J. Behm, Catal. Lett. 76 (2004) 143–150.
[21] L.F. Liotta, G. Pantaleo, F. Puleo, A.M. Venezia, Catal. Today 187 (2012) 10–19.
[22] X. Xu, J. Li, Z. Hao, W. Zhao, C. Hu, Mater. Res. Bull. 41 (2006) 406–413.
[23] A. Beck, A. Horváth, Gy. Stefler, R. Katona, O. Geszti, Gy. Tolnai, L.F. Liotta, L. Guczi, Catal. Today 139 (2008) 180–187.
[24] L. Escamilla-Perea, R. Nava, B. Pawelec, M.G. Rosmaninho, C.L. Peza-Ledesma, J.L.G. Fierro, Appl. Catal. A: Gen. 381 (2010) 42–53.
[25] S. Albonetti, R. Bonelli, R. Delaigle, C. Femoni, E.M. Gaigneaux, V. Morandi, L. Ortolani, C. Tiozzo, S. Zacchini, F. Trifirò, Appl. Catal. A: Gen. 372 (2010) 138–146.
[26] P. Kaminski, M. Ziolek, B. Campo, M. Daturi, Catal. Today (2015) 218–227.
[27] I. Sobczak, K. Szrama, R. Wojcieszak, E.M. Gaigneaux, M. Ziolek, Catal. Today 187 (2012) 48–55.
[28] P. Kaminski, I. Sobczak, P. Decyk, M. Ziolek, W.J. Roth, B. Campo, M. Daturi, J. Phys. Chem. C 117 (2013) 2147–2159.
[29] P. Kaminski, M. Ziolek, J. Catal. 312 (2014) 249–262.
[30] I. Sobczak, T. Wolski, Catal. Today 254 (2015) 72–82.
[31] J. Llorca, M. Domínguez, C. Ledesma, R.J. Chimentão, F. Medina, J. Sueiras, I. Angurell, M. Seco, O. Rossell, J. Catal. 258 (2008) 187–198.
[32] L. Yang, S. Zhou, T. Ding, M. Meng, Fuel Process. Technol. 124 (2014) 155–164.
[33] H. Wu, G. Pantaleo, V. La Parola, A.M. Venezia, X. Collard, C. Aprile, L.F. Liotta, Appl. Catal. B: Environ. 156–157 (2014) 350–361.
[34] E. Smolentseva, A. Simakov, S. Beloshapkin, M. Estrada, E. Vargas, V. Sobolev, R. Kenzhin, S. Fuentes, Appl. Catal. B: Environ. 115–116 (2012) 117–128.
[35] V.V. Galvita, M. Filez, H. Poelman, V. Bliznuk, G.B. Marin, Catal. Lett. 144 (2014) 32–43.
[36] M.S. Aw, I.G. Osojnik Črnivec, A. Pintar, Catal. Sci. Technol. 4 (2014) 1340–1349.
[37] P. Bazin, S. Thomas, O. Marie, M. Daturi, Catal. Today 182 (2012) 3–11.
[38] Y.T. Kim, S.J. You, E.D. Park, Int. J. Hydrogen Energy 37 (2012) 1465–1474.
[39] X. Karatzas, K. Jansson, A. Gonzalez, J. Dawody, L.J. Pettersson, Appl. Catal. B: Environ. 106 (2011) 476–487.
[40] M. Hosseini, S. Siffert, R. Cousin, A. Aboukaïs, Z. Hadj-Sadok, B.-L. Su, C. R. Chim. 12 (2009) 654–659.
[41] H.L. Tidahy, S. Siffert, J.-F. Lamonier, E.A. Zhilinskaya, A. Aboukaïs, Z.-Y. Yuan, A. Vantomme, B.-L. Su, X. Canet, G. De Weireld, M. Frère, T.B. N'Guyen, J.-M. Giraudon, G. Leclercq, Appl. Catal. A: Gen. 310 (2006) 61–69.
[42] V. Idakiev, T. Tabakova, A. Naydenov, Z.-Y. Yuan, B.-L. Su, Appl. Catal. B: Environ. 63 (2006) 178–186.
[43] D. Andreeva, L. Ilieva, V. Idakiev, J.L. Blin, L. Gigot, B.-L. Su, Appl. Catal. A: Gen. 243 (2003) 25–39.
[44] R. Zanella, S. Giorgio, C.R. Henry, C. Louis, J. Phys. Chem. B 106 (2002) 7634–7642.
[45] R. Zanella, L. Delannoy, C. Louis, Appl. Catal. A: Gen. 291 (2005) 62–72.
[46] S.C. Laha, P. Mukerjee, S.R. Sainkar, R. Kumar, J. Catal. 207 (2002) 213–223.
[47] A. Simakov, N. Bogdanchikova, I. Tuzovskaya, E. Smoletseva, A. Pestryakov, M. Farias, M. Avalos, Complex Mediums VI: Light and Complexity, in: M.W. McCall, Graeme Dewar, M.A. Noginov (Eds.), Proc. SPIE, 5924, 2005, p. 101.
[48] I.V. Tuzovskaya, A.V. Simakov, A.N. Pestryakov, N.E. Bogdanchikova, V.V. Gurin, M.H. Farías, H.J. Tiznado, M. Avalos, Catal. Commun. 8 (2007) 977–980.
[49] E. Smolentseva, N. Bogdanchikova, A. Simakov, A. Pestryakov, M. Avalos, M.H. Farias, A. Tompos, V. Gurin, J. Nanosci. Nanotechnol. 7 (2007) 1882–1886.
[50] A.N. Pestryakov, V.V. Lunin, A.N. Kharlanov, D.I. Kochubey, N. Bogdanchikova, A.Yu. Stakheev, J. Mol. Struct. 642 (2002) 129–136.
[51] A.N. Pestryakov, V.V. Lunin, A.N. Kharlanov, N.E. Bogdanchikova, I.V. Tuzovskaya, Eur. Phys. J. D 24 (2003) 307–309.
[52] E. Smolentseva, N. Bogdanchikova, A. Simakov, A. Pestryakov, I. Tuzovskaya, M. Avalos, M.H. Farías, J.A. Díaz, V. Gurin, Surf. Sci. 600 (2006) 4256–4259.
[53] A. Pestryakov, I. Tuzovskaya, E. Smolentseva, N. Bogdanchikova, F. Jentoft, A. Knop-Gericke, Int. J. Mod. Phys. B 19 (2005) 2321–2326.
[54] D.L. Feldheim, C.A. Foss, Metal Nanoparticles: Synthesis, Characterization and Applications, Basel Marcel Dekker Inc., New York, 2002.
[55] V.V. Costa, M. Estrada, Y. Demidova, I. Prosvirin, V. Kriventsov, R.F. Cotta, S. Fuentes, A. Simakov, E.V. Gusevskaya, J. Catal. 292 (2012) 148–156.
[56] R. Feng, M. Li, J. Liu, Colloids Surf. A: Physicochem. Eng. Aspects 406 (2012) 6–12.
[57] C. Guzmán, G. del Ángel, R. Gómez, F. Galindo-Hernández, C. Ángeles-Chavez, Catal. Today 166 (2011) 146–151.
[58] F. Galindo-Hernández, J.A. Wang, R. Gómez, X. Bokhimi, L. Lartundo, A. Mantilla, J. Photochem. Photobiol. A: Chem. 243 (2012) 23–32.
[59] H. Irie, S. Miura, K. Kamiya, K. Hashimoto, Chem. Phys. Lett. 457 (2008) 202–205.

[60] X. Qiu, M. Miyauchi, K. Sunada, M. Minoshima, M. Liu, Y. Lu, D. Li, Y. Shimodaira, Y. Hosogi, Y. Kuroda, K. Hashimoto, ACS Nano 6 (2012) 1609–1618.
[61] K.V.R. Chary, G.V. Sagar, D. Naresh, K.K. Seela, B. Sridhar, J. Phys. Chem. B 109 (2005) 9437–9444.
[62] Z. Liu, M.D. Amiridis, Y. Chen, J. Phys. Chem. B 109 (2005) 1251–1255.
[63] L. Dong, L. Liu, Y. Lv, J. Zhu, H. Wan, B. Liu, F. Gao, X. Wang, J. Mol. Catal. A: Chem. 365 (2012) 87–94.
[64] C. Ampelli, R. Passalacqua, C. Genovese, S. Perathoner, G. Centi, T. Montini, V. Gombac, J.J.D. Jaen, P. Fornasiero, RSC Adv. 3 (2013) 21776–21788.
[65] H.Y. Chen, A. Sayari, A. Adnot, F. Larachi, Appl. Catal. B: Environ. 32 (2001) 195–204.
[66] F. Lin, X. Wu, S. Liu, D. Weng, Y. Huang, Chem. Eng. J. 226 (2013) 105–112.
[67] S. Albonetti, T. Pasini, A. Lolli, M. Blosi, M. Piccinini, N. Dimitratos, J.A. Lopez-Sanchez, D.J. Morgan, A.F. Carley, G.J. Hutchings, F. Cavani, Catal. Today 195 (2012) 120–126.
[68] S. Wu, E.T. Kang, G.K. Neoh, Appl. Surf. Sci. 174 (2001) 296–305.
[69] W. Suprun, M. Lutecki, R. Gläser, H. Papp, J. Mol. Catal. A: Chem. 342–343 (2011) 91–100.
[70] J.F. Moulder, W.F. Stickle, P.E. Sobol, K.D. Bomben, Handbook of X-ray Photoelectron Spectroscopy, Perkin-Elmer Corporation, Physical Electronics Division, Eden Prairie, 1992.
[71] I. Tuzovskaya, N. Bogdanchikova, A. Simakov, V. Gurin, A. Pestryakov, M. Avalos, M.H. Farias, Chem. Phys. 338 (2007) 23–32.
[72] G.M. Veith, A.R. Lupini, S.J. Pennycook, G.W. Ownby, N.J. Dudney, J. Catal. 231 (2005) 151–158.
[73] A.N. Pestryakov, V.V. Lunin, N. Bogdanchikova, O.N. Temkin, E. Smolentseva, Fuel 110 (2013) 48–53.